*Energy Equip. Sys./ Vol. 12/No. 2/June 2024/* 131-151

ENERGY EQUIPSYS

**Energy Equipment and Systems**

www.energyequipsys.com

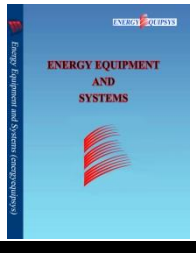


# Thermoeconomic prioritization of heat transfer fluids in solar-driven tri-generation systems using MADM methods

## Manuscript Type

Research Paper

## Authors

**Masood Dehghan**[a]
**Ghasem Akbari** [a*]
**Nader Montazerin**[b]
**Arman Maroufi**[a]

[a] Department of Mechanical Engineering, Qazvin Branch, Islamic Azad University, Qazvin, Iran

[b] Mechanical Engineering Department, Amirkabir University of Technology, Tehran, Iran

*Article history*:

Received : 31 August 2023
Revised : 22 September 2023
Accepted : 8 October 2023

**ABSTRACT**

*Solar heat transfer fluid (HTF) plays a crucial role in the performance of parabolic trough solar collectors (PTSC) and the energy systems integrated with them. In this study, a multi-attribute decision-making (MADM) analysis is employed to prioritize the HTFs for three solar-driven multi-generation energy systems. These systems are based on a direct-fed organic Rankine cycle (ORC) and bottom-cycle arrangement of a double-effect absorption refrigeration cycle and a Kalina cycle system. The ORC configurations include simple, regenerative, and ORC integrated with an internal heat exchanger. The MADM analysis shows that the optimal HTF for all systems is Therminol 66 for which ORC based system demonstrates the best performance in both energy (80.17 %) and exergy (33.21 %) viewpoints. Additionally, this system exhibits the highest performance in terms of net present value (82.6 M$), dynamic payback period (2.19 years) and cost of energy (0.018 $/kWh).*

**Keywords:** MADM; CCHP; Parabolic Trough Solar Collector; Organic Rankine Cycle; Net Present Value; Payback Period; Levelized Cost of Electricity.

## 1. Introduction

Solar-driven multi-generation energy systems are one of the proven technologies to enhance the efficiency of Stand-alone cycles, reduce energy consumption, and the harmful impacts on the environment [1-3]. Parabolic trough collector (PTSC) is the most proven and mature solar thermal technology for power production [4]. Additionally, Solar Heat Transfer Fluid (HTF) plays an important role in the design phase, thermodynamic and economic performance of a PTSC power supply system [5].

Numerous studies have evaluated the HTFs in the PTSC. Mwesigye and Yilmaz [6] conducted a numerical analysis to evaluate the performance of a PTSC system. The results indicate that molten salts exhibit higher thermal performance compared to other synthetic or mineral oils Arslan and Günerhan [7] numerically studied the performance of a PTSC utilizing dowtherm A, solar salt, and pressurized air. The study found that the performance of molten salt was slightly higher. In another numerical study, Okonkwo et al. [8] investigated the performance of six different working fluids: pressurized water, supercritical $CO_2$ ($SC-CO_2$), Therminol VP-1 and oil-based nanofluids containing 3 volumetric ratios

* Corresponding author: Ghasem Akbari
Department of Mechanical Engineering, Qazvin Branch, Islamic Azad University, Nokhbegan Blvd., Qazvin, Iran
E-mail address: g.akbari@qiau.ac.ir

of CuO, $Fe_3O_4$, $Al_2O_3$ dispersed in Therminol VP-1. The study revealed that Therminol VP-1 with $Al_2O_3$ exhibited the highest thermal efficiency. Bellos et al. [9] evaluated the use of the gas working fluids in PTSC systems from a thermodynamic perspective. The results indicated that helium is the optimal choice for inlet temperatures up to 700 K, while carbon dioxide is more suitable for higher temperature levels. The performance of different HTFs (Therminol VP-1, Dowtherm Q, Hitec XL, Helium, and supercritical carbon dioxide) for high-temperature solar thermal applications is examined by Vutukuru et al. [10]. Liquid HTFs exhibit a significantly higher figure of merit compared to gaseous HTFs. Zaharil and Hasanuzzaman [11] performed a thermodynamic analysis of six HTFs (pressurized water, Therminol VP-1, Syltherm 800, Solar Salt, Hitec XL, and liquid Na) under Malaysian climatic conditions. Liquid Na outperformed the other HTFs in terms of thermal efficiency. Thermo-economic comparison of Dowtherm A, Solar Salt, Hitec, and Hitec XL is conducted by Pan et al. [12]. Based on their analysis, solar salt resulted in the lowest levelized cost of electricity (LCOE). Islam et al. [13] investigated the performance of PTSC using three HTFs (ammonia, nitrogen, and carbon dioxide). The maximum collector efficiency was obtained using carbon dioxide.

In terms of using nanofluids, Brahim and Jemni [14] compared the thermal performance of PTSC using Syltherm-800 and Therminol-VP1 non-metallic nanofluids. The Results indicated that Syltherm 800 with CuO and $CeO_2$ nanoparticles were the superior choices. In another study, Ekisiler et al. [15] examined three hybrid nanofluids (Ag–ZnO/Syltherm 800, Ag–$TiO_2$/Syltherm 800, and Ag–MgO/Syltherm 800) while considering three-dimensional turbulent flow conditions. The study reported that the Ag–MgO/Syltherm 800 hybrid nanofluid exhibited the highest thermal efficiency. Bellos and Tzivanidis [16] investigated the use of various nanoparticles (Cu, CuO, $Fe_2O_3$, $TiO_2$, $Al_2O_3$ and $SiO_2$) dispersed in thermal oil (Syltherm 800) in a PTSC. The results indicated that Cu was the most efficient nanoparticle. Mwesigye and Meyer [17] studied the optimum thermal operating conditions of a nanofluid-based PTSC with Cu-Therminol VP-1, Ag-Therminol VP-1 and $Al_2O_3$-Therminol VP-1. They found that Ag-Therminol VP-1 has the highest thermal performance. Comparison tof he thermal efficiency of a PTSC using mono and hybrid nanofluids is performed by Al-Oran et al. [18]. Mono nanoparticles ($Al_2O_3$, $CeO_2$, CuO) and hybrid combinations were dispersed in Syltherm 800. They observed that using $Al_2O_3$was more efficient.

Regarding PTSC-driven power generation systems, Alashkar and Gadalla [19] performed a thermoeconomic analysis of a PTSC-driven power generation system integrated with thermal energy storage, considering Therminol VP-1 and Hitec Solar. The results indicated that Therminol VP-1 and Hitec Solar Salt were the optimal fluids in terms of annual energy output and net annual savings, respectively. In another study, Biencinto et al. [20] conducted an annual yield comparison of PTSC-powered power plants using nitrogen and Therminol VP-1. The results reported that Therminol VP-1 exhibited slightly higher performance from the viewpoint of annual net electrical production. Ramamurathi and Nadar [21] examined the performance of a thermoelectric generator powered by PTSC, considering four HTFs (Therminol VP-1, Therminol XP, $Al_2O_3$-Therminol XP, and CuO-Therminol XP. The results showed that CuO-Therminol XP was the optimal fluid in terms of power generation. Research studies are scarce on the selection and assessment of the HTF in multi-generation energy systems driven by PTSC. In this regard, Assareh et al. [22] evaluated a solar-geothermal cogeneration system, considering Therminol VP-1, Therminol 59, Syltherm 800, and Marlotherm SH as HTFs. The results indicated that Therminol 59 was the optimal fluid in terms of energy efficiency and net output power. However, from the viewpoints of exergy efficiency and LCOE, Therminol VP-1 and Syltherm 800 were identified as the optimal fluids, respectively.

According to the literature reviewed, selection of the HTF for PTSC has been mostly based on one attribute or a set of consistent attributes, which could be challenging, especially in problems in which multiple attributes exhibit different trends. Therefore, the current study utilizes multi-attribute decision-making (MADM) analysis to decide

based on all important criteria of the system, even those with opposite trends. Additionally, despite the significant contribution of HTF to the performance of PTSC-driven power generation systems, there is a shortage of studies on the selection and assessment of HTFs in such systems. Overall, the main contribution of this article is the employment of the MADM analysis to perform assessment and thermoeconomic prioritization of HTF for three novel tri-generation systems involving different organic Rankine cycle (ORC) structures (simple, ORC incorporating internal heat exchanger and regenerative ORC). Organic Rankine cycle (ORC), Kalina cycle system (KCS) and absorption refrigeration cycle (ARC) are integrated into solar power generation systems. This is because of the adaptability of ORC to low and medium-temperature heat sources ($60-350℃$) [23-25], and suitable thermal matching between the heat source and the working fluid temperature profile in the KCS [26]. Additionally, ARC is the most common mode for cooling production in solar-powered energy systems [27, 28].

The article is structured in the following manner. Section 2 outlines the three proposed hybrid systems. Section 3 presents the thermodynamic and economic modeling approach. The MADM analysis is described in section 4. It is followed by validation of the modeling, and presentation and discussion on the results in Sections 5 and 6, respectively.

## Nomenclature

| | |
|---|---|
| A | Area ($m^2$) |
| C | Concentration ratio |
| D | Diameter (m) |
| d | Deviation |
| Ex | Exergy (kJ) |
| $\dot{E}x$ | Exergy rate (kW) |
| F | Focal length (m) |
| G | Solar irradiation ($kW/m^2$) |
| H | hour |
| h | Specific enthalpy ($kJ/kg$) |
| K | Incident angle modifier |
| k | Thermal conductivity ($W/m^2.K$) |
| L | Collector length (m) |
| $\dot{m}$ | Mass flow rate ($kg/s$) |
| P | Pressure |
| $\dot{P}$ | Power rate (kW) |
| Q | Heat (kJ) |
| $\dot{Q}$ | Heat rate (kW) |
| R/r | Normalization value |
| T | Temperature |
| V | Velocity ($m/s$) |
| W | Collector width (m) |
| w | Criterion weight |
| $\dot{W}$ | Electrical power rate (kW) |
| x | Concentration |

**Greek symbols**

| | |
|---|---|
| $\alpha$ | Absorptivity |
| $\gamma$ | Intercept factor |
| $\varepsilon$ | Emissivity |
| $\eta$ | Energy efficiency (%) |
| $\theta$ | Incident angle |
| $\mu$ | Dynamic viscosity ($m^2/s$) |
| $\rho$ | Reflectivity |
| $\sigma$ | Stefan-Boltzmann constant ($W/m^2.K^4$) |
| $\tau$ | Transmissivity |
| $\psi$ | Exergy efficiency (%) |

**Subscripts**

| | |
|---|---|
| ab | Absorber |
| amb | Ambient |
| ap | Aperture |
| b | Beam |
| C | Construction |
| cd | Condenser |
| ci | Cover inner surface |
| co | Cover outer surface |
| coll | Collector |
| con | Concentrator |
| cov | Cover |
| cr | critical |
| el | Electrical |
| eng | Engineering |
| ev | Evaporator |
| max | Maximum |
| opt | Optimum |
| r | Receiver |
| reg | Regenerator |
| ri | Receiver inner surface |
| ro | Receiver outer surface |
| S | Solar |
| t | Total |
| th | Thermal |
| tur | Turbine |
| u | Useful |
| fm | Film |
| g | Generator |
| HP | Heating process |
| in | Inlet |
| loss | Heat losses |
| m | Motor |

**Abbreviation**

| | |
|---|---|
| ARC | Absorption refrigeration cycle |
| CAPEX | Capital Expenditure |
| CCHP | Combined cooling, heat and power |
| CEPCI | Chemical engineering plant cost index |
| COE | Cost of Energy |
| CRF | Capital recovery factor |
| DEARC | Double-effect absorption refrigeration |

| | |
|---|---|
| | cycle |
| DPP | Dynamic payback period |
| EV | Expansion valve |
| FFH | Feed fluid heater |
| GWP | Global warming potential |
| HP | Heating process |
| HPG | High-pressure generator |
| HTF | Heat transfer fluid |
| HTHE | High-temperature heat exchanger |
| IHE | Internal heat exchanger |
| KCS | Kalina cycle system |
| LCOE | Levelized cost of electricity |
| LMTD | Logarithmic mean temperature difference |
| LPG | Low-pressure generator |
| LTHE | Low-temperature heat exchanger |
| MADM | Multy attribute decision making |
| MR | mass flow ratio |
| NOF | Net outranking flow |
| NPV | Net present value |
| Nu | Nusselt number |
| OPEX | Operating expenditure |
| ODP | Ozone depletion potential |
| ORC | Organic Rankine cycle |
| OWF | Organic working fluid |
| Pr | Prandtl number |
| PTSC | Parabolic trough solar collector |
| Re | Reynolds number |
| rev | Revenue |
| RORC | Regenerative organic Rankine cycle |
| SF | Solar field |

## 2. System description

The combined cooling, heating and power (CCHP) systems in the present study, employ the PTSC as the prime mover and utilize the ORC, KCS, heating process unit and DEARC to generate power. Three thermal configurations are proposed in the ORC cycle, namely simple ORC, ORC-IHE and RORC systems. The thermal energy collected by the PTSC is absorbed by the HTF, which supplies the required thermal energy for the ORC and KCS. The heating process (HP) unit and DEARC are directly fed by the ORC. The solar field is made up of 40 rows, each consisting of 17 collectors of LS-2 type. The mass flow rate of the HTF per single row is set to 0.5 kg/s.

### 2.1. ORC based system

The simple ORC system shown in Fig. 1-a, which is based on ORC, operates by pumping the OWF from the outlet of the high-pressure Generator (HPG) (state 32) to the evaporator, where it is utilized to produce power in the turbine. The heat required for the HP unit and the HPG is supplied by the fluid exiting the turbine (state 35).

The ORC-IHE based system (Fig. 1-b) incorporates an intermediate heat exchanger (IHE). Initially, the fluid leaving the HPG (state 32) is pumped to the IHE for preheating before proceeding to the evaporator and turbine. The fluid exiting the turbine (state 36) provides heat to the IHE and, after being discharged from it, supplies the required thermal energy for the HP and DEARC systems.

The regenerative ORC (RORC) based system (Fig. 1-c) includes a feed fluid heater (FFH). The fluid leaving the HPG (state 32) is directed to the FFH where it is combined with the high-pressure vapor coming out of the turbine (state 37). This combined stream is then pumped towards the evaporator and turbine. The low-pressure vapor at the outlet of the turbine (state 38) provides the necessary heat for the HP and DEARC systems.

### 2.2. Kalina cycle

All three CCHP systems illustrated in Fig. 1 employ the KCS11-type Kalina cycle. In the KCS system, the working fluid absorbs heat from the HTF in the evaporator (state 5). It then separates into two phases: rich ammonia-water saturated vapor (state 6) for power generation and poor ammonia-water saturated liquid (state 7) for regeneration. The poor ammonia-water liquid undergoes a throttling process (state 10) and is subsequently mixed with the expanded rich ammonia-water from the turbine (state 8). The fluid leaving the condenser (state 12) is then pumped towards the regenerator for pre-heating and directed back to the evaporator to complete the cycle.

### 2.3. Double effect Absorption refrigeration cycle

All tri-generation systems employ a double effect LiBr-H2O absorption chiller that operates in a series-flow configuration, as shown in Fig. 1. The weak solution leaving the absorber (state 28) is pre-heated by passing through the low and high temperature heat exchanger (LTHE and HTHE) before entering the HPG (state 31). In the HPG, a portion of water evaporates, producing primary

refrigerant vapor (state 15) and medium solution (state 22). The medium solution then goes through HTHE and the expansion valve EV-4 before entering the low-pressure generator (LPG). In the LPG, the primary refrigerant vapor condenses (state 16), creating secondary refrigerant vapor (state 18) and strong solution (state 25). The condensed primary refrigerant vapor mixes with the secondary refrigerant vapor in the condenser after passing through valve EV-2. The refrigerant then enters the evaporator at a lower temperature due to heat rejection in the condenser and throttling in valve EV-1 (state 20). Finally, the strong solution passes through LTHE and expansion valve EV-3 before mixing with the refrigerant vapor (state 21) in the absorber to produce the weak solution (state 28).

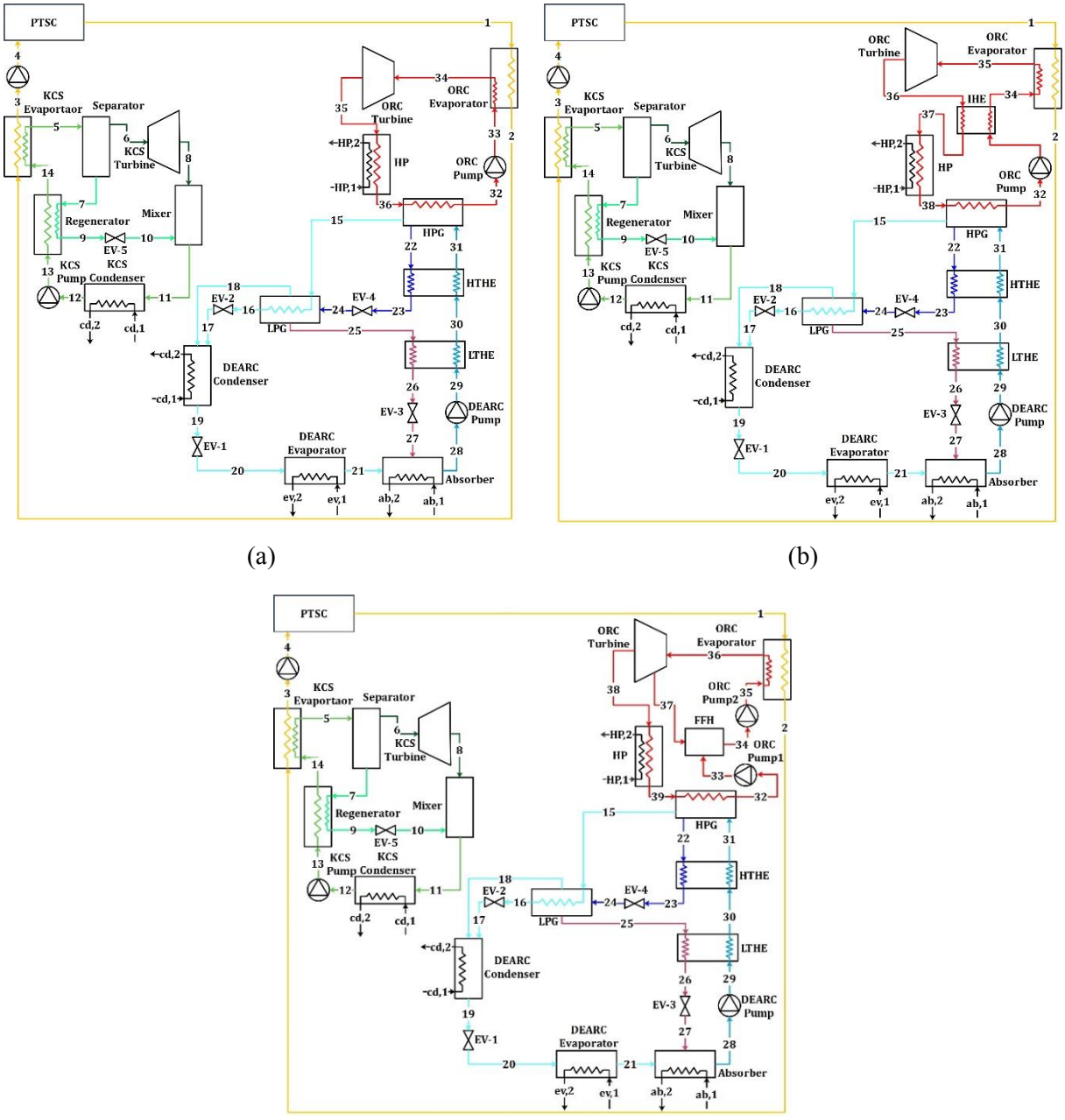


**Fig. 1.** Schematic representation of the ORC based (a), ORC-IHE based (b) and RORC based (c) trigeneration systems.

### 2.4. General methodology and assumptions

The present study aims to perform multi-criteria optimization of the HTF for three proposed CCHP systems by utilizing the MADM method based on thermodynamic and economic characteristics. In this manner, the input data (as listed in Tables 1, 2, and 3) are set, and the purchase cost equations of various system components are employed to calculate thermodynamic and economic performance metrics. Subsequently, the PROMETHEE II scheme, a MADM technique, combined with Shannon's entropy method is utilized for thermoeconomic prioritization of the HTF considering different OWFs. Additionally, the Golden Section Search method is employed to determine the optimal mass flow ratio of OWF and HTF. A numerical code is developed in MATLAB® to solve the governing equations and post-process the results. It is linked with the Engineering Equation Solver (EES®) to extract thermodynamic properties. The assumptions considered in this study are as follows:

- Steady-state operation
- Dead state pressure and temperature of 101.325 kPa and 298.15 K, respectively
- Negligible pressure drop and friction in the piping system and heat exchangers
- Minimal changes of kinetic and potential energy/exergy
- Pre-defined isentropic efficiencies for pumps and turbines
- Saturated liquid state at condensers outlet and saturated vapor state at evaporators outlet
- Discarding chemical exergy of the working fluid in the DEARC [29]
- The mixture temperature at the separator inlet of the KCS is 30℃ less than the dew point temperature.

## 3. Mathematical modeling

### 3.1. Parabolic trough solar collector

Considering $T_{in}$ as the HTF temperature at the receiver inlet and $T_{amb}$ as the ambient temperature, the useful heat gain is obtained using [30]

$$\dot{Q}_u = K_1\dot{Q}_s - K_2(T_{in}^4 - T_{amb}^4). \quad (1)$$

The values for coefficients $K_1$ and $K_2$ are determined using the data provided in Table 4, and $\dot{Q}_S$ refers to solar beam irradiation, which is defined as

$$\dot{Q}_S = A_{ap}G_b, \quad (2)$$

where $A_{ap}$ and $G_b$ denote the collector aperture area and solar beam intensity, respectively. Considering $\dot{Q}_u$ as the thermal input, and performing energy balance on the solar collector, the HTF outlet temperature is obtained using[30]

$$T_{out} = T_{in} + \dot{Q}_S\left(\frac{K_4}{\dot{m}c_P}\right) - \left(\frac{K_5}{\dot{m}c_P}\right)\left({T_{in}}^4 - {T_{amb}}^4\right), \quad (3)$$

where $c_P$ and $\dot{m}$ are constant-pressure specific heat and mass flow rate of HTF, respectively.

**Table 1.** Input data for PTSC [30, 31].

| Parameter | Symbol | Value | Parameter | Symbol | Value |
|---|---|---|---|---|---|
| Geometrical parameters | | | | | |
| Width | $W$ | 5 m | Length | $L$ | 7.8 m |
| Focal length | $F$ | 1.71 m | Concentration ratio | $C$ | 22.74 |
| Receiver inner area | $A_{ri}$ | 1.617 $m^2$ | Receiver outer area | $A_{ro}$ | 1.715 $m^2$ |
| Cover inner area | $A_{ci}$ | 2.671 $m^2$ | Cover outer area | $A_{co}$ | 2.818 $m^2$ |
| Receiver inner diameter | $D_{ri}$ | 0.066 m | Receiver outer diameter | $D_{ro}$ | 0.070 m |
| Cover inner diameter | $D_{ci}$ | 0.109 m | Cover outer diameter | $D_{co}$ | 0.115 m |
| Aperture area | $A_{ap}$ | 39 $m^2$ | Number of rows | $N_r$ | 40 |
| Optical/operating parameters | | | | | |
| Receiver emittance | $\varepsilon_r$ | 0.2 | Cover emittance | $\varepsilon_{cov}$ | 0.9 |
| Receiver absorptivity | $\alpha$ | 0.96 | Cover transmissivity | $\tau$ | 0.95 |
| Intercept factor | $\gamma$ | 0.99 | Concentrator reflectivity | $\rho_{con}$ | 0.83 |
| Incident angle | $\theta$ | 0° | Incident angle modifier | $K(\theta = 0°)$ | 1 |
| Maximum optical efficiency | $\eta_{opt,max}$ | 75% | Solar beam intensity | $G_b$ | 650 $W/m^2$ |
| HTF mass flow rate at each row | $\dot{m}_{HTF}$ | 0.5 kg/s | HTF temperature at the collector inlet | $T_4$ | 55 ℃ |

**Table 2.** Input data for ORC (three types), DEARC and KCS [32-34].

| Cycle/Parameter | Value | Cycle/Parameter | Value |
|---|---|---|---|
| **ORC/KCS** | | **DEARC** | |
| Turbine isentropic efficiency | 0.9 | HPG temperature | 120 ℃ |
| Pump isentropic efficiency | 0.9 | Condenser temperature | 35 ℃ |
| Electrical generator efficiency | 0.95 | Absorber temperature | 35 ℃ |
| Electrical motor efficiency | 0.95 | Evaporator temperature | 7 ℃ |
| Regenerator effectiveness | 0.75 | LPG pinch point temperature | 5 ℃ |
| ORC turbine inlet pressure | 2000 kPa | Effectiveness of heat exchangers | 0.7 |
| ORC feed fluid heater pressure | 500 kPa | Solution pump efficiency | 0.95 |
| ORC pump inlet temperature | 123 ℃ | | |
| KCS condenser temperature | 30 ℃ | | |
| KCS separator inlet pressure | 35 | | |
| $NH_3$ concentration at KCS separator inlet | 0.9 | | |

**Table 3.** Input data for economic analysis [35]

| Parameter | Definition | Value |
|---|---|---|
| d | Discount rate | 5 (%) |
| N | Project life time | 25 (year) |
| $C_{el}$ | Electrical cost | 0.214 ($/kWh) |
| $C_h$ | Heating cost | 0.107 ($/kWh) |
| $C_c$ | Cooling cost | 0.071 ($/kWh) |

**Table 4.** Definition of coefficients $\boldsymbol{K_1}$ to $\boldsymbol{K_5}$ used in the PTSC modelling [30, 31].

| Coefficient | Definition |
|---|---|
| $K_1$ * | $\eta_{opt}\left[1+\frac{4T_{in}^{\ 3}K_3}{K_4}\right]^{-1}$ |
| $K_2$ | $K_3\left[1+\frac{4T_{in}^{\ 3}K_3}{K_4}\right]^{-1}$ |
| $K_3$ ** | $A_{ro}\varepsilon_r^*\sigma\left[1+\frac{4T_{amb}^{\ 3}A_{ro}\varepsilon_r^*\sigma}{K_5}\right]^{-1}$ |
| $K_4$ *** | $\left[\frac{1}{h_{fm}A_{ri}}+\frac{1}{2\dot{m}c_P}\right]^{-1}$ |
| $K_5$ | $A_{co}\varepsilon_{cov}\sigma T_{amb}^{\ 3}+A_{co}h_{cov,o}$ |

* $\eta_{opt}$ is optimal efficiency of the collector, expressed as $\eta_{opt}=K(\theta)\rho_{con}\gamma\tau\alpha$, where $K(\theta)$ represents the incident angle modifier coefficient, given as [36]: $K(\theta)=1-2.2307\times10^{-4}\theta-1.1\times10^{-4}\theta^2+3.18596\times10^{-6}\theta^3-4.85509\times10^{-8}\theta^4$

** $\varepsilon_r^*$ in definition of $K_3$ is expressed as $\varepsilon_r^*=\left[\frac{1}{\varepsilon_r}+\frac{1-\varepsilon_c}{\varepsilon_c}\left(\frac{A_{ro}}{A_{ri}}\right)\right]^{-1}$

*** $h_{fm}$ is convective heat transfer coefficient for the flow inside the absorber pipe, expressed as $h_{fm}=0.023k\left(Re^{0.8}Pr^{0.4}\right)/D_{ri}$ [30].

### 3.2. Thermodynamic performance of tri-generation systems

The thermodynamic performance of the tri-generation systems is evaluated by utilizing the overall net electrical, heating, and cooling powers, as well as the overall energy and exergy efficiencies. The overall net electrical power for cycles or multi-generation system is calculated as [37]

$$\dot{W}_{net,overall}=\sum\dot{W}_{tur}\eta_g-\sum\frac{\dot{W}_{pump}}{\eta_m} \quad (4)$$

where $\eta_g$ and $\eta_m$ are the efficiencies of the electrical generator and pump electromotor, respectively.

The heating power generated by the HP unit ($\dot{Q}_{heating}$) and the cooling power produced by DEARC ($\dot{Q}_{cooling}$) are calculated as

$$\dot{Q}_{heating} = \dot{m}_{HP}^{ORC}\left(h_{HP,in}^{ORC} - h_{HP,out}^{ORC}\right) \quad (5)$$

$$\dot{Q}_{cooling} = \dot{m}_{ev}^{DEARC}\left(h_{ev,out}^{DEARC} - h_{ev,in}^{DEARC}\right), \quad (6)$$

where $\dot{m}_{HP}^{ORC}$ and $\dot{m}_{ev}^{DEARC}$ represent mass flow rates of HP unit and DEARC evaporator, respectively.

The overall energy and exergy efficiencies are, respectively, given by [32, 37]

$$\eta_{CCHP} = \frac{\dot{W}_{net,overall} + \dot{Q}_{heating} + \dot{Q}_{cooling}}{\dot{Q}_{in}}, \quad (7)$$

*and*

$$\Psi_{CCHP} = \frac{\dot{W}_{net,overall} + \dot{E}x_{heating} + \dot{E}x_{cooling}}{\dot{E}x_{coll}}, \quad (8)$$

where $\dot{Q}_{in}$ is the input (solar) energy and $\dot{E}x_{coll}$ is the collector exergy, which is calculated as [37]

$$\dot{E}x_{coll} = A_{ap,t} G_b \left(1 + \left(\frac{1}{3}\right)\left(\frac{T_0}{T_{sun}}\right)^4 - \left(\frac{4}{3}\right)\left(\frac{T_0}{T_{sun}}\right)\right) \quad (9)$$

where $T_0$ is surrounding temperature and $T_{sun}$ is the sun temperature (6000 K) [37]. Also, heating exergy in the HP unit and cooling exergy in the DEARC evaporator ($\dot{E}x_{heating}$ and $\dot{E}x_{cooling}$) are given by [38]

$$\dot{E}x_{heating} = \dot{m}_{HP}\left(ex_{HP,out} - ex_{HP,in}\right), \quad (10)$$

*and*

$$\dot{E}x_{heating} = \dot{m}_{HP}\left(ex_{HP,out} - ex_{HP,in}\right), \quad (11)$$

where $T_{ev}^{DEARC}$ is the temperature of the DEARC evaporator.

### 3.3. Economic Modeling of tri-generation system

The economic performance of the CCHP systems is examined by considering NPV, DPP, LCOE and cost of energy (COE). Several important parameters including capital expenditure (CAPEX), operation and maintenance expenditure (OPEX), annual revenue (rev) and net revenue ($rev_{net}$) are involved.

CAPEX and OPEX are expressed as [39, 40]

$$CAPEX = Z_{eq,t} + Z_c + Z_{con} + Z_{eng} \quad and \quad (12)$$

$$OPEX = 0.06 CRF.CAPEX \quad (13)$$

The total equipment purchase cost ($Z_{eq,t}$) is determined by the thermodynamic and geometrical factors outlined in Table 5. However, the costs of the separator, mixer, and expansion valve are significantly lower than the other components, so they have been excluded from consideration [41, 42]). In addition, civil and construction ($Z_c$), contingency ($Z_{con}$), and engineering and supervision ($Z_{eng}$) costs are calculated as [39, 40]

$$Z_c = 0.2\ Z_{eq,t} \quad (14)$$

$$Z_{con} = 0.15\ Z_{eq,t} \quad (15)$$

$$Z_{eng} = 0.15\left(Z_{eq,t} + Z_c + Z_{con}\right) \quad (16)$$

The capital recovery factor ($CRF$) is determined by taking into account the discount rate ($d$) and the project's lifetime ($N$) using [43]

$$CRF = \frac{d\left(1+d\right)^N}{\left(1+d\right)^N - 1} \quad (17)$$

The CEPCI as a modifier coefficient is employed to update the costs to the present year based on the values obtained from Table 6 at the base year, expressed as [44]

$$Cost\ at\ present\ year = Original\ cost \times \frac{CEPCI_{\ present\ year}}{CEPCI_{\ base\ year}} \quad (18)$$

For the base years 2000, 2005, 2010, 2012 and 2015 (as listed in Table 6) and 2023 as the present year, CEPCI is 394.1, 468.2, 550.8, 584.6, 556.8 and 798, respectively [45]. The area of heat exchangers is the main parameter for the assessment of their costs (Table 6), which is calculated as [39]

$$A_k = \frac{\dot{Q}_k}{U_K . LMTD_K} \quad (19)$$

where $\dot{Q}_k$ is heat transfer rate and $U_K$ is the overall heat transfer coefficient, as presented in Table 6. The logarithmic mean temperature difference (LMTD) for each heat exchanger is given by

$$LMTD = \frac{\left(T_{h,in} - T_{c,out}\right) - \left(T_{h,out} - T_{c,in}\right)}{ln\left(\frac{T_{h,in} - T_{c,out}}{T_{h,out} - T_{c,in}}\right)} \quad (20)$$

where the indices $h$ and $c$ stand for hot and cold streams, respectively.

The $rev$ and $rev_{net}$ of the plant are calculated as [35]

$$rev = \sum \dot{P} \cdot H \cdot C, \quad (21)$$

$$rev_{net} = rev - OPEX, \quad (22)$$

where $\dot{P}$ and $C$ notifies the power production rate and its cost, respectively, and H indicates annual operating hour that is considered as 3285 hours in this study.

Finally, NPV, DPP, COE and LCOE are [35, 46, 47]:

$$NPV = -CAPEX + \sum_{i=1}^{N} \frac{rev_{net,i}}{(1+d)^{i}} \quad (23)$$

$$DPP = ln\left(\frac{1}{1-\frac{CAPEX.d}{rev_{net}}}\right).(ln(1+d))^{-1} \quad (24)$$

$$LCOE = \frac{CRF \cdot CAPEX + OPEX}{\dot{W}_{net,overall} \cdot H} \quad (25)$$

$$COE = \frac{CRF \cdot CAPEX + OPEX}{(\dot{W}_{net,overall} + \dot{Q}_{heating} + \dot{Q}_{cooling}) \cdot H} \quad (26)$$

**Table 5.** Purchase cost equations for various components of trigeneration systems [39, 48, 49]

| Equipment | Cost equation | base year |
|---|---|---|
| Solar cycle | | |
| PTSC | $Z_{PTSC} = 170A_{ap}$ | 2015 |
| Pump | $Z_{pump} = 1120(\dot{W}_{pump})^{0.8}$ | 2012 |
| ORC/KCS | | |
| Turbine | $Z_{tur} = 4405(\dot{W}_{tur})^{0.7}$ | 2012 |
| Pump | $Z_{pump} = 1120(\dot{W}_{pump})^{0.8}$ | 2012 |
| HE | $Z_{HE} = 130\left(\frac{A_{HE}}{0.093}\right)^{0.78}$ | 2005 |
| Evaporator | $Z_{ev} = 130\left(\frac{A_{ev}}{0.093}\right)^{0.78}$ | 2005 |
| Condenser | $Z_{cd} = 1773\dot{m}_{vapor}$ | 2010 |
| **DEARC** | | |
| Evaporator/ Absorber | $Z_{ev/ab}^{DEARC} = 16000\left(\frac{A_{ev/ab}^{DEARC}}{100}\right)^{0.6}$ | 2000 |
| Condenser | $Z_{cd}^{DEARC} = 8000\left(\frac{A_{cd}^{DEARC}}{100}\right)^{0.6}$ | 2000 |
| Generator | $Z_{gen}^{DEARC} = 17500\left(\frac{A_{gen}^{DEARC}}{100}\right)^{0.6}$ | 2000 |
| Pump | $Z_{pump}^{DEARC} = 2100\left(\frac{\dot{W}_{pump}^{DEARC}}{10}\right)^{0.26}\left(\frac{(1-\eta_{pump}^{DEARC})}{\eta_{pump}^{DEARC}}\right)^{0.5}$ | 2000 |
| HE | $Z_{HE}^{DEARC} = 12000\left(\frac{Z_{HE}^{DEARC}}{100}\right)^{0.6}$ | 2000 |

**Table 6.** Overall heat transfer coefficient of heat exchangers [39, 50]

| Parameter | Value $(\frac{KW}{m^2K})$ | Parameter | Value $(\frac{KW}{m^2K})$ | Parameter | Value $(\frac{KW}{m^2K})$ | Parameter | Value $(\frac{KW}{m^2K})$ |
|---|---|---|---|---|---|---|---|
| $U_{ev}$ | 1.5 | $U_{HE}$ | 1 | $U_{ev}^{DEARC}$ | 1.1 | $U_{cd}^{DEARC}$ | 0.5 |
| $U_{cd}$ | 1.1 | $U_{gen}^{DEARC}$ | 1.3 | $U_{ab}^{DEARC}$ | 0.8 | $U_{HE}^{DEARC}$ | 0.7 |

## 4. Multi-attribute decision-making analysis

MADM approaches aim to identify optimal outcomes in intricate problems encompassing multiple criteria and conflicting objectives [51]. These techniques have extensive usage in various research topics regarding energy systems including optimization [52,53], location selection [54], technology prioritization [55-58],

resource selection [59, 60], and energy policy-making [61].

The process of prioritizing HTFs along with the optimal selection of OWFs is a complex decision-making problem that involves different thermodynamic and economic criteria and objectives with different trends. Applying MADM methods to this problem provides a reliable approach [62]. In this manner, PROMETHEE (preference ranking organization method for enrichment evaluation) [63] is utilized as a MADM technique. PROMETHEE is considered one of the most efficient outranking methods for addressing multi-criteria problems and has been widely utilized in energy applications [64-68]. The PROMETHEE I provides a partial ranking of alternatives, while PROMETHEE II, an enhanced version, establishes explicit priorities among the alternatives [69, 70]. The outranking principle is employed to rank the alternatives, and a pairwise comparison of the alternatives is conducted to determine their rankings based on a comprehensive evaluation criterion known as the net outranking flow (NOF) [71]. This approach is particularly appropriate for problems with a limited number of alternatives that need to be assessed using multiple criteria [69, 72, 73]. Due to the explicit ranking ability of the PROMETHEE II, and also a finite number of alternatives in this study (the candidate HTFs and OWFs), this method is applied.

Shannon's entropy method is employed to determine the weight of thermodynamic and economic criteria. The basis of this technique is the theory of entropy, in which criteria with lower entropy values are more informative and are assigned higher weights [74]. Figs 2 and 3 schematically represent procedures of the PROMETHEE II method [75] and Shannon's entropy [76].

### 4.1. HTF selection

Thermal oils are the most widely used HTFs in PTSC plants due to their well-established and advanced technology, as well as their commercial availability. They have a lifespan of over 30 years, low vapor pressure, and are reasonably priced [5, 77, 78]. Therefore, the current study employs thermal oils as the HTF. Based on the physical and thermodynamic properties of PTSC and the solar field, as well as the maximum usage temperature of the HTF, four fluids, namely Therminol vp1, Therminol 66, Therminol xp and Syltherm 800 are selected as the HTF. The properties of these fluids are summarized in Table 7.

### 4.2. OWF selection

The initial selection of OWFs is performed considering environmental aspects and thermodynamic limitations. Several criteria are used for this purpose, as follows:

1. In accordance with the Kyoto and Montreal Protocols, fluids with high global warming potential (GWP) and ozone depletion potential (ODP) are being phased out. Therefore, fluids with GWP lower than 150 [79] and zero ODP are considered.
2. The critical temperature and pressure of OWF must be higher than the minimum temperature and maximum pressure in the ORC cycle.
3. The operating temperature range of the ORC cycle should be in the stability temperature range of each selected OWF.
4. In order to avoid the adverse effect of moisture on the turbine blades and efficiency, a dry turbine exit is ensured. [80].

Regarding the above environmental and thermodynamic criteria, Table 8 presents the list of selected OWFs for the optimization process.

The evaluation of different thermodynamic and economic parameters revealed that maximizing the ORC evaporator heat absorption capacity ($\dot{Q}_{ev}^{ORC}$) is the key quantity to achieving the highest performance of the tri-generation system (see section 6.1). Additionally, improving the mass flow ratio of the OWF and HTF (MR) has a direct impact on $\dot{Q}_{ev}^{ORC}$. Therefore, an optimization process is conducted to identify the optimal MR with $\dot{Q}_{ev}^{ORC}$ as the objective function. In this regard, the Golden Section search method is utilized to optimize the $MR_{opt}$ considering $0.5 \leq MR \leq 2.5$ . The constraint in determining the maximum value of $\dot{Q}_{ev}^{ORC}$ is the minimum outlet temperature of HTF evaporator, which should not be lower than the sum of the OWF

evaporator inlet temperature and pinch point temperature. This technique sequentially narrows a search interval to determine the minimum or maximum value of a unimodal function. The search step size across the entire process is the golden ratio ($(\sqrt{5}-1)/2$) [81].

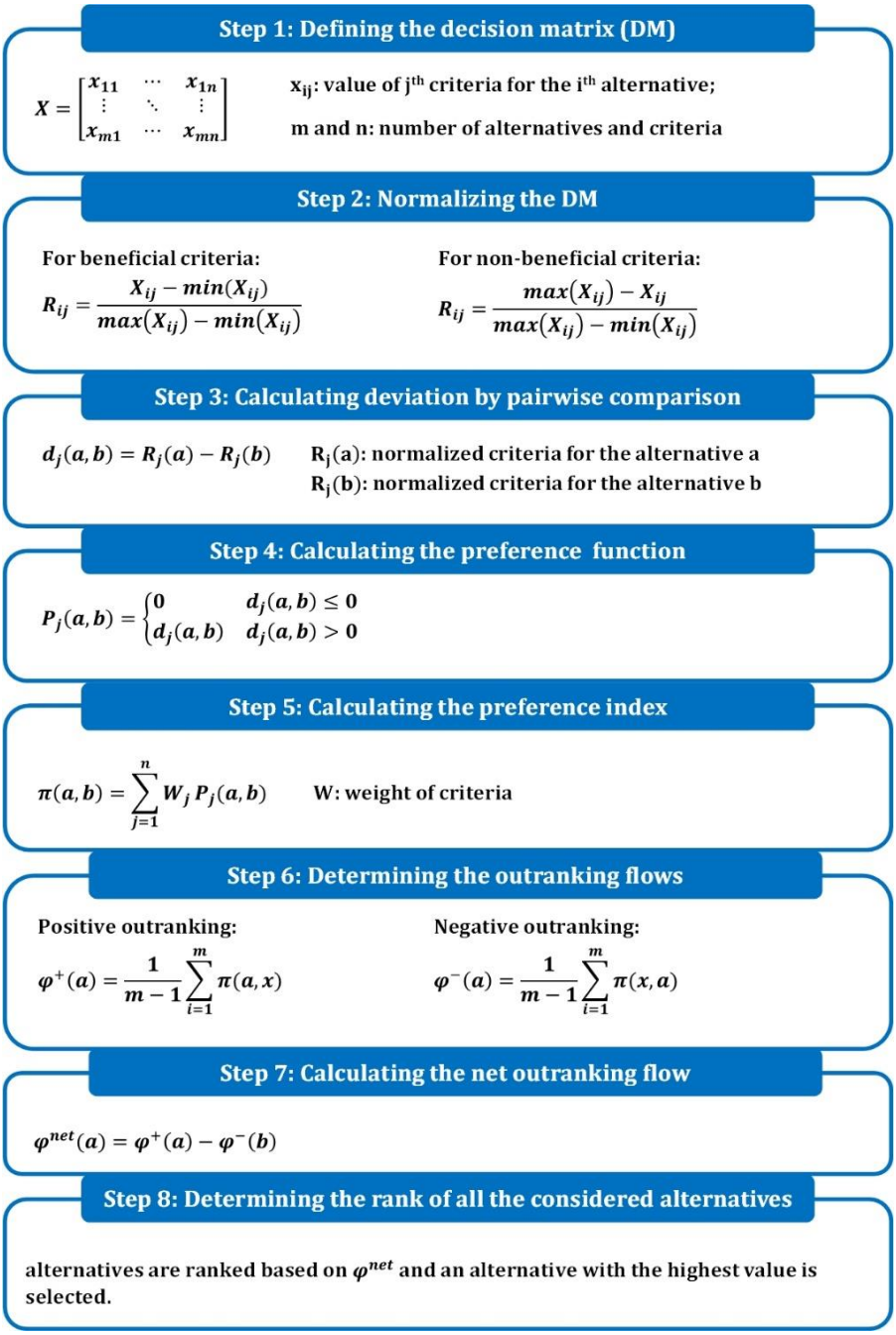


**Fig. 2.** Procdure of PROMETHEE II method

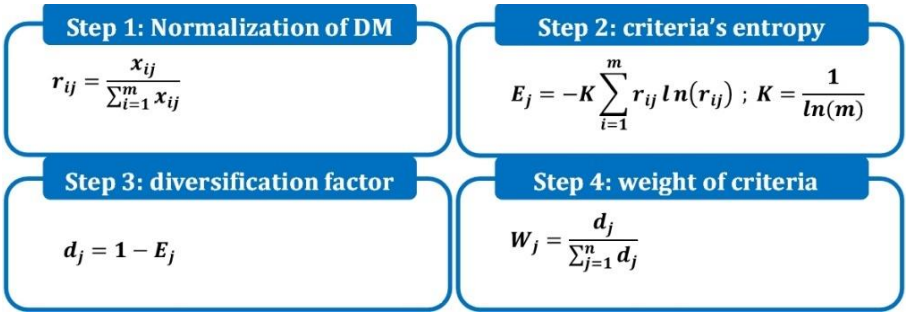


**Fig. 3.** Procedure of Shannon's entropy method

**Table 7.** Thermodynamic properties of selected HTFs [28, 82]

| Parameters | HTF | | | |
|---|---|---|---|---|
| | Therminol vp1 | Therminol 66 | Therminol xp | Syltherm 800 |
| Density at 25℃ | 1060 kg/m$^3$ | 1005 kg/m$^3$ | 875 kg/m$^3$ | 936 kg/m$^3$ |
| Normal boiling point | 257 ℃ | 359 ℃ | 358 ℃ | 400 |
| Temperature range (Recommended) | 12 to 400 ℃ | -3 to 345 ℃ | -20 to 315 ℃ | -40 to 400 ℃ |

**Table 8.** Primary ORC fluids selected for the optimization stage based on environmental and thermodynamic aspects

| Fluids | $T_C$(℃) | $P_C(KPa)$ | ODP | GWP |
|---|---|---|---|---|
| N-Pentane*, ** | 196.5 | 3364 | 0 | 4 |
| Isohexane*, ** | 224.6 | 3040 | 0 | 3 |
| N-Hexane | 234.7 | 3058 | 0 | 3 |
| N-Heptane | 267 | 2727 | 0 | 3 |
| Cyclohexane | 280.5 | 4081 | 0 | 4 |
| N-Octane | 296.2 | 2497 | 0 | 3 |
| Benzene | 288.9 | 4894 | 0 | 3.4 |
| Toluene | 318.6 | 4126 | 0 | 3.3 |
| p-Xylene | 343 | 3532 | 0 | 3 |
| Ethylbenzene | 344 | 3622 | 0 | 3 |

* These fluids are not selected for RORC system, because of unrealistic results ($P_{33} < P_{32}$).
** Regarding thermal stability condition of ORC, N-pentane are not selected when HTF is Therminol vp1 and Syltherm 800, and Isohexane just considered for Therminol xp.

### 4.3. Decision-making criteria

The current study considers a set of main thermodynamic and economic criteria as decision parameters. Overall energy and exergy efficiencies, overall net electrical, heating, and cooling power are selected as thermodynamic criteria, along with NPV, DPP, COE, and LCOE as economic metrics. These metrics are introduced in Section 3.

## 5. Validation

The modeling precision of the PTSC, ORCs, and KCS in this study is evaluated by comparing them with the work of Dudley et al. [83], Safarian and Aramoun [84], and He et al. [85], respectively (Tables 9-11). The comparison is conducted under the same conditions and operating characteristics as reported in the literature. The outcomes notify a good agreement in terms of the relative error. In addition, to validate the modeling of the DEARC, an integrated DEARC with a CCHP system [32] is utilized. By applying the same input heat from the ORC to the DEARC and maintaining similar operating conditions, the COP calculated by the current model is 1.18, which is precisely the same as the value reported in [32].

**Table 9.** Verification of the results obtained for the PTSC system with the experimental results of Dudley et al. [83].

| | Input data | | | | Results & errors | | | | | |
|---|---|---|---|---|---|---|---|---|---|---|
| | | | | | $T_{out}$(K) | | | $\eta_{en}$(%) | | |
| | $G_b$ ($\frac{W}{m^2}$) | $T_{amb}$ (K) | $T_{in}$ (K) | $\dot{V}$ ($\frac{L}{min}$) | Present study | Ref. value | Relative error (%) | Present study | Ref. value | Relative Error (%) |
| 1 | 933.7 | 294.35 | 375.35 | 47.7 | 397.6 | 397.15 | 0.11 | 73.13 | 72.51 | 0.85 |
| 2 | 968.2 | 295.55 | 424.15 | 47.8 | 447 | 446.45 | 0.12 | 72.25 | 70.9 | 1.90 |
| 3 | 982.3 | 297.45 | 470.65 | 49.1 | 493.1 | 492.65 | 0.09 | 71.18 | 70.17 | 1.43 |
| 4 | 909.5 | 299.35 | 523.85 | 54.7 | 542.5 | 542.55 | 0.009 | 69.4 | 70.25 | 1.21 |
| 5 | 937.9 | 301.95 | 570.95 | 55.5 | 590 | 590.05 | 0.008 | 67.54 | 67.98 | 0.64 |
| 6 | 903.2 | 304.25 | 629.05 | 56.3 | 647.3 | 647.15 | 0.02 | 64.11 | 63.82 | 0.45 |
| 7 | 920.9 | 302.65 | 652.65 | 56.8 | 671.3 | 671.15 | 0.02 | 62.62 | 62.34 | 0.44 |

**Table 10.** Verification of the results obtained for the three ORC-based cycles with the results reported by Safarian and Aramoun [84]. The input data is: $T_{cd} = 25$℃; $P_{ev} = 2.5$ MPa; $P_{FFH} = 1$ MPa; $\eta_{tur} = 0.8$; $\eta_{pump} = 0.85$

| Cycle | $\eta_{el}$ (%) | | |
|---|---|---|---|
| | Present study | Ref. value | Relative error (%) |
| ORC | 19.63 | 19.46 | 0.8 |
| ORC-IHE | 21.7 | 21.5 | 0.9 |
| RORC | 22.4 | 22 | 1.8 |

**Table 11.** Verification of the results obtained for the KCS cycle with the results reported by He et al. [85].

| Input data | | Results & errors | | |
|---|---|---|---|---|
| | | $\eta_{el}$ (%) | | |
| $P_1(MPa)$ | $X_1$ | Present study | Ref. value | Relative error (%) |
| 1.5 | 0.59 | 8.02 | 7.97 | 0.6 |
| 2 | 0.69 | 8.62 | 8.46 | 1.8 |
| 2.5 | 0.81 | 9.34 | 9.19 | 1.6 |
| 3 | 0.92 | 10.28 | 10.23 | 0.4 |

## 6. Results and discussion

Firstly, this section presents the thermoeconomic prioritization of HTFs using the MADM approach. Then, the tri-generation systems are examined in terms of their economic and thermodynamic characteristics. The input data for modeling ORCs, KCS and DEARC are summarized in Table 2.

### 6.1. Thermoeconomic Prioritization of HTF

In this paper, the MADM results are exclusively presented for the selection of HTFs, with the deliberate exclusion of OWFs to maintain the paper's conciseness. Because of the enhancement of thermodynamic and economic characteristics with an increase of $\dot{Q}_{ev}^{ORC}$ (as shown in Fig. 4) and due to the direct impact of MR on the $\dot{Q}_{ev}^{ORC}$, the optimal value of MR is first determined for the tri-generation systems for different HTFs and OWFs, as listed in Table 12. Additionally, prior to the multi-criteria selection of HTF for each system, the optimal OWF is determined based on the optimum value of MR using the MADM approach, as presented in Table 13.

The optimal HTFs for tri-generation systems are determined by the PROMETHEE method based on the net outranking flow (NOF). The NOF provides an overall measure of the superiority of an alternative compared to others from a multi-criteria thermo-economic perspective. Fig. 5 presents the calculated NOF of selected HTFs for different tri-generation systems based on the optimal OWFs and MR. Multi-criteria optimization of HTF indicates that the maximum NOF for all systems is obtained by Therminol 66. In the other words, Therminol 66 results in the highest overall performance in a multi-criteria thermo-economic viewpoint.

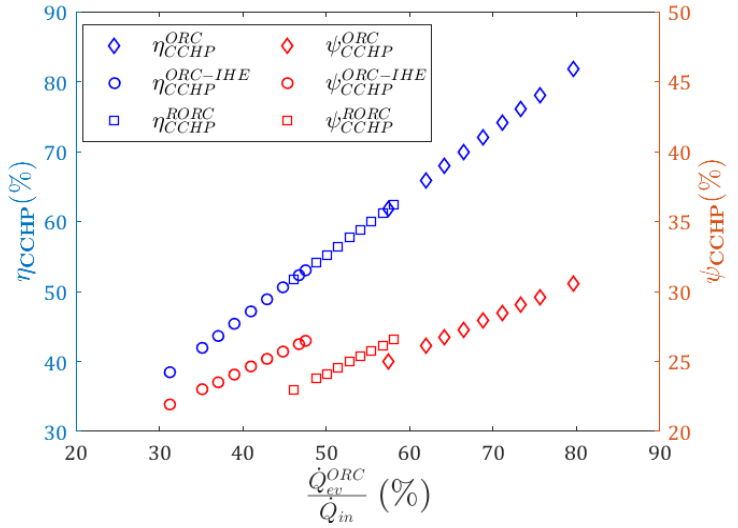


(a)

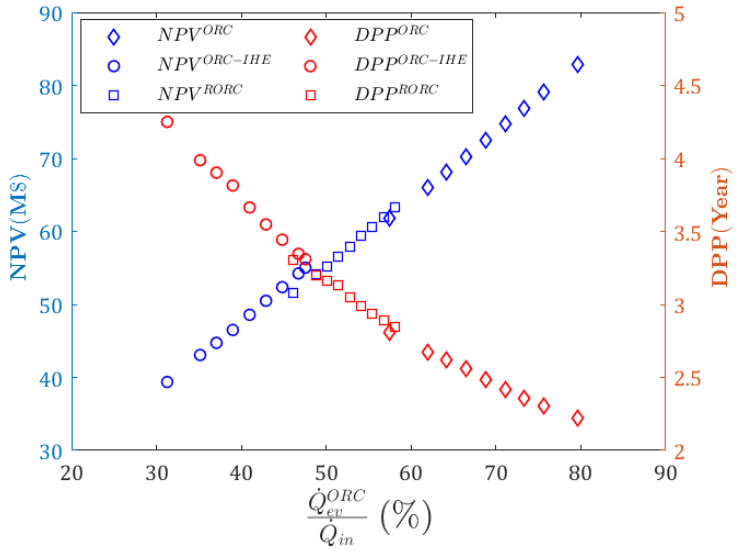


(b)

**Fig. 4.** Effect of ORC evaporator heat absorption on the thermodynamic and economic characteristics. (HTF: Therminol vp1, OWF: N-octane)

**Table 12.** Optimum MR for the candidate OWFs for different HTFs

The missing values are for the fluids that are filtered out at specific conditions, as in the footnote of Table 8.

| OWF | ORC based system | | | | ORC-IHE based system | | | | RORC based system | | | |
|---|---|---|---|---|---|---|---|---|---|---|---|---|
| | $HTF_1$ | $HTF_2$ | $HTF_3$ | $HTF_4$ | $HTF_1$ | $HTF_2$ | $HTF_3$ | $HTF_4$ | $HTF_1$ | $HTF_2$ | $HTF_3$ | $HTF_4$ |
| N-Pentane | ----- | 1.12 | 1.30 | ----- | 1.91 | 2.06 | 1.73 | 1.65 | ----- | ----- | ----- | ----- |
| Isohexane | ----- | ----- | 1.36 | ----- | 1.37 | 1.45 | 1.12 | 1.19 | ----- | ----- | ----- | ----- |
| N-Hexane | 1.06 | 1.23 | 1.42 | 0.87 | 1.16 | 1.23 | 1.28 | 1.02 | 1.05 | 1.22 | 1.41 | 0.86 |
| N-Heptane | 1.07 | 1.26 | 1.41 | 0.87 | 0.98 | 1.22 | 1.37 | 0.66 | 1.04 | 1.25 | 1.38 | 0.85 |
| Cyclohexane | 1.21 | 1.41 | 1.50 | 1.00 | 1.14 | 1.37 | 1.50 | 0.79 | 1.19 | 1.40 | 1.50 | 0.99 |
| N-Octane | 1.09 | 1.29 | 0.48 | 0.89 | 1.03 | 1.27 | 0.48 | 0.83 | 1.05 | 1.27 | 1.50 | 0.85 |
| Benzene | 1.41 | 1.65 | 1.29 | 1.17 | 1.39 | 1.64 | 1.29 | 1.14 | 1.39 | 1.65 | 1.29 | 1.16 |
| Toluene | 1.42 | 1.35 | 0.62 | 1.16 | 1.40 | 1.35 | 0.62 | 1.14 | 1.38 | 1.35 | 0.62 | 1.13 |
| P-xylene | 0.91 | 0.65 | 0.62 | 0.94 | 0.91 | 0.65 | 0.62 | 0.94 | 0.91 | 0.65 | 0.62 | 0.94 |
| Ethylbenzene | 0.92 | 0.68 | 0.62 | 0.94 | 0.92 | 0.68 | 0.62 | 0.94 | 0.92 | 0.68 | 0.62 | 0.94 |

$(HTF_1, HTF_2, HTF_3, HTF_4) = (\text{Therminol VP1}, \text{Therminol 66}, \text{Therminol XP}, \text{Syltherm 800})$

**Table 13.** Optimal OWFs selected for three tri-generation systems for different HTFs

| HTF | Trigeneration system | | |
|---|---|---|---|
| | ORC based system | ORC-IHE based system | RORC based system |
| Therminol VP1 | Toluene | Toluene | Benzene |
| Syltherm 800 | Toluene | Toluene | Benzene |
| Therminol 66 | Benzene | Benzene | Benzene |
| Therminol XP | N-Heptane | Cyclohexane | N-hexane |

6.2. Performances of tri-generation systems

The results presented in this section are based on the optimal HTF obtained in section 6.1. The input energy and exergy ($\dot{Q}_{in}$ and $\dot{E}x_{coll}$) are the same in all systems. Table 14 presents thermodynamic and economic performance characteristics of different systems. In terms of heating and cooling, ORC based system is superior, while in terms of overall net electrical power, ORC-IHE based system is the best. The results indicate that ORC based system leads to the highest performance in both energy and exergy efficiencies (80.17 % and 33.21 %, respectively). This is because of significant heating power and exergy in the heating process of the ORC-based system compared to the other hybrid systems. In terms of economic characteristics like NPV, DPP and COE, ORC based system leads to the best performance, since it has the highest overall output power (17385.7 kW). Additionally, ORC-IHE based system outperforms other systems in terms of LCOE.

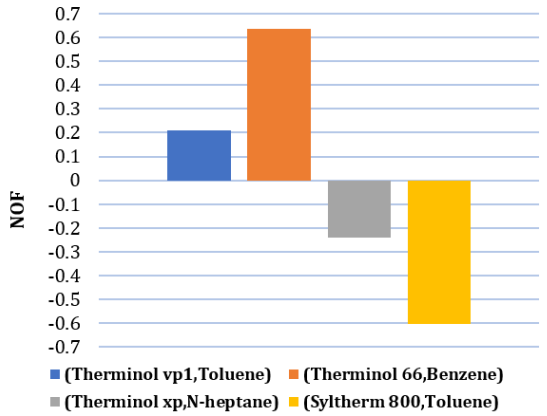


(a)

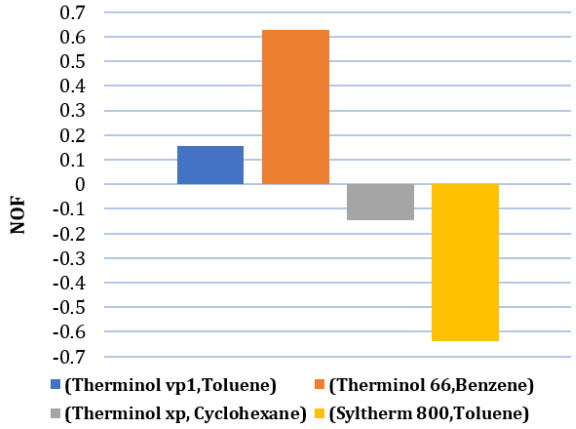


(b)

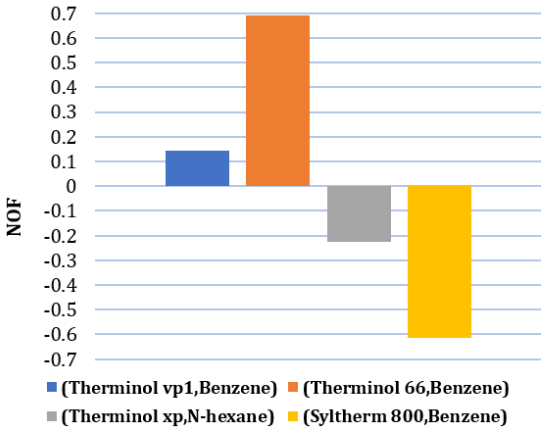


(c)

**Fig. 5.** NOF of selected HTFs: (a) ORC based; (b) ORC-IHE based; (c) RORC based

**Table 14.** Thermodynamic and economic performance of tri-generation systems

| Metrics | ORC based | ORC-IHE based | RORC based |
|---|---|---|---|
| $\psi_{CCHP}$ (%) | 33.21 | 32.01 | 32.25 |
| $\eta_{CCHP}$ (%) | 80.17 | 71.89 | 74.42 |
| $\dot{W}_{net,overall}$ (kW) | 2702.4 | 2909.9 | 2801.9 |
| $\dot{Q}_{heating}$ (kW) | 13383.0 | 11388.5 | 12156.6 |
| $\dot{Q}_{cooling}$ (kW) | 1297.3 | 1289.4 | 1176.3 |
| NPV (M$) | 82.6 | 74.5 | 77.0 |
| LCOE ($/kwh) | 0.118 | 0.111 | 0.114 |
| DPP (year) | 2.19 | 2.45 | 2.35 |
| COE ($/kWh) | 0.018 | 0.021 | 0.020 |

**Table 15.** Comparison of economic characteristics of the present systems with those of literature

| Metric | Present systems | | | Literature | |
|---|---|---|---|---|---|
| | ORC based | ORC-IHE based | RORC based | Ref. | Amount |
| COE ($/kwh) | 0.018 | 0.021 | 0.020 | [86] | 0.023 |
| LCOE ($/kwh) | 0.118 | 0.111 | 0.114 | [87] | 0.25 |

In order to compare the performance of present system with literature in a multi-criteria approach, COE and LCOE are employed and the results are presented in Table 15. It is evident that the current configurations lead to greater performance. Such enhancement is mainly because of higher efficiency of the present systems compared to the literature (46.3 and 25% for [86] and [87], respectively).

## 7. Conclusions

This study applied the MADM method based on multiple thermodynamic and economic criteria for the prioritization of HTFs in PTSC-driven energy systems. The investigated systems consisted of PTSC as the prime mover, different types of ORC system directly fed by a solar field, and DEARC and KCS as two bottoming cycles. The PROMETHEE II method combined with the Shannon's entropy scheme was utilized for multi-criteria selection of HTFs. Overall energy and exergy efficiencies, overall net electrical, heating, and cooling power, NPV, DPP, COE, and LCOE were selected as thermodynamic and economic criteria.

Considering thermophysical properties of the PTSC and the solar field, as well as the maximum allowable temperature of each HTF, Therminol vp1, Therminol 66, Therminol xp and Syltherm 800 were selected. MADM analysis of the systems was carried out in terms of net outranking flow to evaluate them in a multi-criteria thermoeconomic viewpoint. Therminol 66 was found as the optimal HTF leading to the highest overall performance for all three trigeneration systems.

Based on the optimal HTF, the ORC based system demonstrated the best performance in terms of heating and cooling powers, as well as both energy and exergy efficiencies (80.17 % and 33.21 %, respectively). Additionally, this system exhibited the highest performance in terms of NPV (82.6 M$), DPP (2.19 year) and COE (0.018 $/kWh). In contrast, ORC-IHE based system resulted in the highest overall net electrical power and LCOE (0.111 $/kWh).

## References

[1] Wu, D. and R. Wang, Combined cooling, heating and power: A review. progress in energy and combustion science, 2006. 32(5-6): p. 459-495.

[2] Kialashaki, Y., A linear programming optimization model for optimal operation strategy design and sizing of the CCHP systems. Energy Efficiency, 2018. 11: p. 225-238.

[3] Haghghi, M.A., et al., Thermodynamic assessment of a novel multi-generation solid oxide fuel cell-based system for production of electrical power, cooling, fresh water, and hydrogen. Energy conversion and management, 2019. 197: p. 111895.

[4] Ehyaei, M., et al., Energy, exergy and economic analyses for the selection of working fluid and metal oxide nanofluids in a parabolic trough collector. Solar Energy, 2019. 187: p. 175-184.
[5] Yılmaz, İ.H., A. Mwesigye, and F. Kılıç, Prioritization of heat transfer fluids in parabolic trough solar systems using CFD-assisted AHP-VIKOR approach. Renewable Energy, 2023. 210: p. 751-768.
[6] Mwesigye, A. and İ.H. Yılmaz, Thermal and thermodynamic benchmarking of liquid heat transfer fluids in a high concentration ratio parabolic trough solar collector system. Journal of Molecular Liquids, 2020. 319: p. 114151.
[7] Arslan, F.M. and H. Günerhan. Investigation of energetic and exergetic performances of parabolic trough collector with using different heat transfer fluids. in E3S Web of Conferences. 2019. EDP Sciences.
[8] Okonkwo, E.C., M. Abid, and T.A. Ratlamwala, Numerical analysis of heat transfer enhancement in a parabolic trough collector based on geometry modifications and working fluid usage. Journal of Solar Energy Engineering, 2018. 140(5): p. 051009.
[9] Bellos, E., et al., The use of gas working fluids in parabolic trough collectors–An energetic and exergetic analysis. Applied Thermal Engineering, 2016. 109: p. 1-14.
[10] Vutukuru, R., A.S. Pegallapati, and R. Maddali, Suitability of various heat transfer fluids for high temperature solar thermal systems. Applied Thermal Engineering, 2019. 159: p. 113973.
[11] Zaharil, H. and M. Hasanuzzaman, Modelling and performance analysis of parabolic trough solar concentrator for different heat transfer fluids under Malaysian condition. Renewable Energy, 2020. 149: p. 22-41.
[12] Pan, C.A., et al. Identification of optimum molten salts for use as heat transfer fluids in parabolic trough CSP plants. A techno-economic comparative optimization. in AIP Conference Proceedings. 2018. AIP Publishing.
[13] Islam, M., M. Hasanuzzaman, and N. Rahim, Modelling and analysis of the effect of different parameters on a parabolic-trough concentrating solar system. RSC advances, 2015. 5(46): p. 36540-36546.
[14] Brahim, T. and A. Jemni, Comparative Study of Parabolic Trough Solar Collector using Syslterm-800 and Therminol-VP1 Non-metallic Nanofluids. Thermal Science and Engineering Progress, 2023: p. 101951.
[15] Ekiciler, R., et al., Effect of hybrid nanofluid on heat transfer performance of parabolic trough solar collector receiver. Journal of Thermal Analysis and Calorimetry, 2021. 143: p. 1637-1654.
[16] Bellos, E. and C. Tzivanidis, Thermal efficiency enhancement of nanofluid-based parabolic trough collectors. Journal of Thermal Analysis and Calorimetry, 2019. 135: p. 597-608.
[17] Mwesigye, A. and J.P. Meyer, Optimal thermal and thermodynamic performance of a solar parabolic trough receiver with different nanofluids and at different concentration ratios. Applied Energy, 2017. 193: p. 393-413.
[18] Al-Oran, O., F. Lezsovits, and A. Aljawabrah, Exergy and energy amelioration for parabolic trough collector using mono and hybrid nanofluids. Journal of Thermal Analysis and Calorimetry, 2020. 140: p. 1579-1596.
[19] Alashkar, A. and M. Gadalla. Evaluation of thermal energy storage (TES) systems on thermo-economic characteristics of PTSC solar-based power generation plants. in ASME International Mechanical Engineering Congress and Exposition. 2018. American Society of Mechanical Engineers.
[20] Biencinto, M., et al., Performance model and annual yield comparison of parabolic-trough solar thermal power plants with either nitrogen or synthetic oil as heat transfer fluid. Energy conversion and management, 2014. 87: p. 238-249.
[21] Ramamurthi, P.V. and E.R. Samuel Nadar, An integrated SiGe based thermoelectric generator with parabolic trough collector using nano HTF for effective harvesting of solar radiant energy. Journal of Electronic Materials, 2019. 48: p. 7780-7791.
[22] Assareh, E., et al., A Transient simulation for a novel solar-geothermal cogeneration system with a selection of heat transfer

fluids using Thermodynamics analysis and ANN intelligent (AI) modeling. Applied Thermal Engineering, 2023: p. 120698.
[23] Guo, J., X. Huai, and Z. Liu, Performance investigation of parabolic trough solar receiver. Applied Thermal Engineering, 2016. 95: p. 357-364.
[24] Li, P., et al., A cascade organic Rankine cycle power generation system using hybrid solar energy and liquefied natural gas. Solar Energy, 2016. 127: p. 136-146.
[25] Shuang, Y., et al., ANALYSIS OF HEAT TRANSFER AND IRREVERSIBILITY OF ORGANIC RANKINE CYCLE EVAPORATOR FOR SELECTING WORKING FLUID AND OPERATING CONDITIONS. Thermal Science, 2020. 24.
[26] Wang, Y., et al., Thermodynamic performance comparison between ORC and Kalina cycles for multi-stream waste heat recovery. Energy Conversion and Management, 2017. 143: p. 482-492.
[27] Bi, Y., et al., Performance analysis of solar air conditioning system based on the independent-developed solar parabolic trough collector. Energy, 2020. 196: p. 117075.
[28] Shirazi, A., et al., Solar-powered absorption chillers: A comprehensive and critical review. Energy Conversion and Management, 2018. 171: p. 59-81.
[29] Avanessian, T. and M. Ameri, Energy, exergy, and economic analysis of single and double effect LiBr–H2O absorption chillers. Energy and Buildings, 2014. 73: p. 26-36.
[30] Bellos, E. and C. Tzivanidis, Analytical expression of parabolic trough solar collector performance. Designs, 2018. 2(1): p. 9.
[31] Al-Oran, O., F. Lezsovits, and A. Aljawabrah, Exergy and energy amelioration for parabolic trough collector using mono and hybrid nanofluids. Journal of Thermal Analysis and Calorimetry, 2020: p. 1-18.
[32] Eisavi, B., et al., Thermodynamic analysis of a novel combined cooling, heating and power system driven by solar energy. Applied Thermal Engineering, 2018. 129: p. 1219-1229.
[33] Ghaebi, H., et al., Energy, exergy and exergoeconomic analysis of a cogeneration system for power and hydrogen production purpose based on TRR method and using low grade geothermal source. Geothermics, 2018. 71: p. 132-145.
[34] Gogoi, T. and P. Hazarika, Comparative assessment of four novel solar based triple effect absorption refrigeration systems integrated with organic Rankine and Kalina cycles. Energy Conversion and Management, 2020. 226: p. 113561.
[35] Zarei, A., et al., Energy, exergy and economic analysis of a novel solar driven CCHP system powered by organic Rankine cycle and photovoltaic thermal collector. Applied Thermal Engineering, 2021. 194: p. 117091.
[36] Haghghi, M.A., et al., Thermodynamic investigation of a new combined cooling, heating, and power (CCHP) system driven by parabolic trough solar collectors (PTSCs): A case study. Applied Thermal Engineering, 2019. 163: p. 114329.
[37] Al-Sulaiman, F.A., I. Dincer, and F. Hamdullahpur, Exergy modeling of a new solar driven trigeneration system. Solar Energy, 2011. 85(9): p. 2228-2243.
[38] Bellos, E., C. Tzivanidis, and K.A. Antonopoulos, Parametric investigation and optimization of an innovative trigeneration system. Energy Conversion and Management, 2016. 127: p. 515-525.
[39] Dehghani, M.J. and C.K. Yoo, Modeling and extensive analysis of the energy and economics of cooling, heat, and power trigeneration (CCHP) from textile wastewater for industrial low-grade heat recovery. Energy Conversion and Management, 2020. 205: p. 112451.
[40] Ifaei, P., J. Rashidi, and C. Yoo, Thermoeconomic and environmental analyses of a low water consumption combined steam power plant and refrigeration chillers–Part 1: Energy and economic modelling and analysis. Energy Conversion and Management, 2016. 123: p. 610-624.
[41] Gebreslassie, B.H., et al., Design of environmentally conscious absorption cooling systems via multi-objective optimization and life cycle assessment. Applied Energy, 2009. 86(9): p. 1712-1722.
[42] Shokati, N., F. Ranjbar, and M. Yari, Exergoeconomic analysis and optimization of basic, dual-pressure and dual-fluid ORCs

and Kalina geothermal power plants: A comparative study. Renewable Energy, 2015. 83: p. 527-542.
[43] Wang, S., et al., Thermo-economic evaluations of dual pressure organic Rankine cycle (DPORC) driven by geothermal heat source. Journal of Renewable and Sustainable Energy, 2018. 10(6).
[44] Habibi, H., et al., Thermo-economic performance evaluation and multi-objective optimization of a screw expander-based cascade Rankine cycle integrated with parabolic trough solar collector. Applied Thermal Engineering, 2020. 180: p. 115827.
[45] Tzivanidis, C. and E. Bellos, The use of parabolic trough collectors for solar cooling–A case study for Athens climate. Case Studies in Thermal Engineering, 2016. 8: p. 403-413.
[46] Tzivanidis, C., E. Bellos, and K.A. Antonopoulos, Energetic and financial investigation of a stand-alone solar-thermal Organic Rankine Cycle power plant. Energy conversion and management, 2016. 126: p. 421-433.
[47] Chen, H., et al., Thermodynamic and economic analyses of a solar-aided biomass-fired combined heat and power system. Energy, 2021. 214: p. 119023.
[48] Kurup, P. and C.S. Turchi, Parabolic trough collector cost update for the system advisor model (SAM). 2015, National Renewable Energy Lab.(NREL), Golden, CO (United States).
[49] Haghghi, M.A., et al., Exergoeconomic evaluation of a system driven by parabolic trough solar collectors for combined cooling, heating, and power generation; a case study. Energy, 2020. 192: p. 116594.
[50] Chen, K., et al., Thermodynamic and economic comparison of novel parallel and serial combined cooling and power systems based on sCO2 cycle. Energy, 2021. 215: p. 119008.
[51] Kumar, A., et al., A review of multi criteria decision making (MCDM) towards sustainable renewable energy development. Renewable and Sustainable Energy Reviews, 2017. 69: p. 596-609.
[52] Sun, Z., C. Liu, and S. Wang, Multi-objective decision framework for comprehensive assessment of organic Rankine cycle system. Journal of Renewable and Sustainable Energy, 2020. 12(1).
[53] Liu, J., et al., Optimal selection of energy storage nodes based on improved cumulative prospect theory in China. Journal of Renewable and Sustainable Energy, 2020. 12(6).
[54] Wang, C.-N., et al., Multi-criteria decision making (MCDM) approaches for solar power plant location selection in Viet Nam. Energies, 2018. 11(6): p. 1504.
[55] He, C., et al., Combined cooling heating and power systems: Sustainability assessment under uncertainties. Energy, 2017. 139: p. 755-766.
[56] Ren, J., Multi-criteria decision making for the prioritization of energy systems under uncertainties after life cycle sustainability assessment. Sustainable Production and Consumption, 2018. 16: p. 45-57.
[57] Saryazdi, S.M.E., et al., Multi-objective optimization of preheating system of natural gas pressure reduction station with turbo-expander through the application of waste heat recovery system. Thermal Science and Engineering Progress, 2023. 38: p. 101509.
[58] Khan, M.A., A. Ali, and M. Zakaria, Analysis of power plants in China Pakistan economic corridor (CPEC): An application of analytic network process (ANP). Journal of Renewable and Sustainable Energy, 2018. 10(6).
[59] Chalvatzis, K.J., et al., Sustainable resource allocation for power generation: The role of big data in enabling interindustry architectural innovation. Technological Forecasting and Social Change, 2019. 144: p. 381-393.
[60] Yazdani, M., et al., A novel integrated decision-making approach for the evaluation and selection of renewable energy technologies. Clean Technologies and Environmental Policy, 2018. 20: p. 403-420.
[61] Alizadeh, R., et al., Improving renewable energy policy planning and decision-making through a hybrid MCDM method. Energy Policy, 2020. 137: p. 111174.
[62] Ilbahar, E., S. Cebi, and C. Kahraman, A state-of-the-art review on multi-attribute

renewable energy decision making. Energy Strategy Reviews, 2019. 25: p. 18-33.
[63] Brans, J.-P. and P. Vincke, Note—A Preference Ranking Organisation Method: (The PROMETHEE Method for Multiple Criteria Decision-Making). Management science, 1985. 31(6): p. 647-656.
[64] Diakoulaki, D. and F. Karangelis, Multi-criteria decision analysis and cost–benefit analysis of alternative scenarios for the power generation sector in Greece. Renewable and sustainable energy reviews, 2007. 11(4): p. 716-727.
[65] Goumas, M. and V. Lygerou, An extension of the PROMETHEE method for decision making in fuzzy environment: Ranking of alternative energy exploitation projects. European Journal of Operational Research, 2000. 123(3): p. 606-613.
[66] Haralambopoulos, D. and H. Polatidis, Renewable energy projects: structuring a multi-criteria group decision-making framework. Renewable energy, 2003. 28(6): p. 961-973.
[67] Madlener, R., K. Kowalski, and S. Stagl, New ways for the integrated appraisal of national energy scenarios: The case of renewable energy use in Austria. Energy policy, 2007. 35(12): p. 6060-6074.
[68] Wang, J.-J., et al., Review on multi-criteria decision analysis aid in sustainable energy decision-making. Renewable and sustainable energy reviews, 2009. 13(9): p. 2263-2278.
[69] Alinezhad, A. and J. Khalili, New methods and applications in multiple attribute decision making (MADM). Vol. 277. 2019: Springer.
[70] Özkale, C., et al., Decision analysis application intended for selection of a power plant running on renewable energy sources. Renewable and sustainable energy reviews, 2017. 70: p. 1011-1021.
[71] Khanlari, A. and M. Alhuyi Nazari, A review on the applications of multi-criteria decision-making approaches for power plant site selection. Journal of Thermal Analysis and Calorimetry, 2021: p. 1-17.
[72] Cavallaro, F., Multi-criteria decision aid to assess concentrated solar thermal technologies. Renewable Energy, 2009. 34(7): p. 1678-1685.
[73] Strantzali, E., K. Aravossis, and G.A. Livanos, Evaluation of future sustainable electricity generation alternatives: The case of a Greek island. Renewable and Sustainable Energy Reviews, 2017. 76: p. 775-787.
[74] Lee, H.-C. and C.-T. Chang, Comparative analysis of MCDM methods for ranking renewable energy sources in Taiwan. Renewable and sustainable energy reviews, 2018. 92: p. 883-896.
[75] Ozsahin, I., D.U. Ozsahin, and B. Uzun, Applications of multi-criteria decision-making theories in healthcare and biomedical engineering. 2021: Academic Press.
[76] Saraswat, S. and A.K. Digalwar, Evaluation of energy alternatives for sustainable development of energy sector in India: An integrated Shannon's entropy fuzzy multi-criteria decision approach. Renewable Energy, 2021. 171: p. 58-74.
[77] Moya, E.Z., Innovative working fluids for parabolic trough collectors, in Advances in concentrating solar thermal research and technology. 2017, Elsevier. p. 75-106.
[78] Awan, A.B., et al., Commercial parabolic trough CSP plants: Research trends and technological advancements. Solar Energy, 2020. 211: p. 1422-1458.
[79] Wang, S., et al., Selection principle of working fluid for organic Rankine cycle based on environmental benefits and economic performance. Applied Thermal Engineering, 2020. 178: p. 115598.
[80] Mondragon, R., et al., Advances in New Heat Transfer Fluids From Numerical to Experimental Techniques. Chapter 11-New High-Temperature Heat Transfer and Thermal Storage Molten Salt–Based Nanofluids Preparation, Stabilization, and Characterization. 2017, Taylor & Francis Group, LLC.
[81] Syltherm®heat transfer fluids. Technical bulletin, available at:. <www.dow.com>.
[82] Pejic, D. and M. Arsic, Minimization and maximization of functions: golden-section search in one dimension. Exploring the DataFlow Supercomputing Paradigm: Example Algorithms for Selected Applications, 2019: p. 55-90.
[83] Dudley, V.E., et al., Test results: SEGS LS-2 solar collector. 1994, Sandia National

Lab.(SNL-NM), Albuquerque, NM (United States).

[84] Safarian, S. and F. Aramoun, Energy and exergy assessments of modified Organic Rankine Cycles (ORCs). Energy reports, 2015. 1: p. 1-7.

[85] He, J., et al., Performance research on modified KCS (Kalina cycle system) 11 without throttle valve. Energy, 2014. 64: p. 389-397.

[86] Tariq, S., U. Safder, and C. Yoo, Exergy-based weighted optimization and smart decision-making for renewable energy systems considering economics, reliability, risk, and environmental assessments. Renewable and Sustainable Energy Reviews, 2022. 162: p. 112445.

[87] Tozlu, A., B. Gençaslan, and H. Özcan, Thermoeconomic analysis of a hybrid cogeneration plant with use of near-surface geothermal sources in Turkey. Renewable Energy, 2021. 176: p. 237-250.